

# Probing top-quark couplings indirectly at Higgs factories

Gauthier Durieux<sup>1</sup> Jiayin Gu (顾嘉荫)<sup>2</sup> Eleni Vryonidou<sup>3</sup> Cen Zhang (张岑)<sup>4</sup>

<sup>1</sup> DESY Notkestraße 85, D-22607, Hamburg, Germany

<sup>2</sup> PRISMA Cluster of Excellence, Institut für Physik,

Johannes Gutenberg-Universität, 55099 Mainz, Germany

<sup>3</sup> Theoretical Physics Department, CERN, 1211 Geneva 23, Switzerland

<sup>4</sup> Institute of High Energy Physics, and School of Physical Sciences,  
University of Chinese Academy of Sciences, Beijing 100049, China

**Abstract:** We perform a global effective-field-theory analysis to assess the combined precision on Higgs couplings, triple gauge-boson couplings, and top-quark couplings, at future circular  $e^+e^-$  colliders, with a focus on runs below the  $t\bar{t}$  production threshold. Deviations in the top-quark sector entering as one-loop corrections are consistently taken into account in Higgs and diboson processes. We find that future lepton colliders running at center-of-mass energies below the  $t\bar{t}$  production threshold can still provide useful information on top-quark couplings, by measuring virtual top-quark effects. With rate and differential measurements, the indirect individual sensitivity achievable is better than at the high-luminosity LHC. However, strong correlations between the extracted top-quark and Higgs couplings are also present and lead to much weaker global constraints on top-quark couplings. This implies that a direct probe of top-quark couplings above the  $t\bar{t}$  production threshold is helpful also for the determination of Higgs and triple-gauge-boson couplings. In addition, we find that below the  $e^+e^- \rightarrow t\bar{t}h$  production threshold, the top-quark Yukawa coupling can be determined by its loop corrections to all Higgs production and decay channels. Degeneracy with the  $ggh$  coupling can be resolved, and even a global limit is competitive with the prospects of a linear collider above the threshold. This provides an additional means of determining the top-quark Yukawa coupling indirectly at lepton colliders.

**Key words:** effective field theory, top quark, lepton collider

**PACS:** 13.66.Fg, 14.65.Ha, 14.80.Bn

## 1 Introduction

After the discovery of the Higgs boson [1, 2], understanding the electroweak symmetry breaking mechanism remains one of the major challenges in particle physics. The determination of Higgs couplings at the Large Hadron Collider (LHC) is now approaching, and in some cases surpassing, the 10% precision level. Improvements beyond this level can be foreseen at proposed  $e^+e^-$  colliders. These machines could run at a center-of-mass energy of 240–250 GeV—where the maximum of the  $e^+e^- \rightarrow hZ$  cross section lies—or even above, and would provide a much cleaner environment for precision determination of Higgs couplings. Prospects have been widely studied through global analyses in the standard-model effective field theory (SMEFT) and revealed that improvements of up to several orders of magnitude can be achieved compared to present limits [3–9].

Given the expected precision of measurements at future lepton colliders, next-to-leading-order (NLO) theory predictions in the SMEFT can potentially be relevant.

These corrections can involve effective operators which do not appear at leading order, and therefore provide new opportunities in the exploration of physics beyond the standard model (SM). The indirect determination of the trilinear Higgs self-coupling, which enters single Higgs production and decay processes at one loop, has for instance already been studied [8–10].

Effective operators which give rise to anomalous  $tbW$ ,  $ttZ$ ,  $tt\gamma$  and  $t\bar{t}h$  couplings of the top quark can also become relevant at one loop. If future lepton colliders run above the  $e^+e^- \rightarrow t\bar{t}$  and  $t\bar{t}h$  production thresholds, these operator coefficients will be determined by direct measurements (see Ref. [11] for a recent global study of top-quark operators at future lepton colliders). Yet, at lower center-of-mass energies, they enter in loop corrections to other electroweak processes. Recently, it has been pointed out that these corrections are not negligible already at the LHC [12]. Runs of future lepton colliders below the  $t\bar{t}$  and  $t\bar{t}h$  production thresholds may thus still provide complementary information on top-quark couplings.

<sup>1</sup> E-mail: gauthier.durieux@desy.de

<sup>2</sup> E-mail: jiagu@uni-mainz.de

<sup>3</sup> E-mail: eleni.vryonidou@cern.ch

<sup>4</sup> E-mail: cenzhang@ihep.ac.cn

plings.

Moreover, the top quark is an indispensable player in Higgs coupling analyses due to its large Yukawa coupling. Already in the SM, several important channels are dominated by its loop contributions. Deviations which would be observed there could be sourced by the anomalous top-quark couplings. However, it has been stressed in Ref. [5] that NLO SMEFT predictions for processes that are not loop-induced in the SM are necessary for a global and consistent fit at that order. Fortunately, computations at NLO in the electroweak gauge couplings have become available for Higgs processes in the past few years [13–19]. In particular, the NLO corrections involving top-quark operators for Higgs processes have become available very recently [12], making such a combined analysis feasible at future lepton colliders. The only missing ingredient was the theory prediction for  $W^+W^-$  production at the same order. This process is notably sensitive to the triple gauge-boson couplings (TGC) which can be generated by operators affecting also Higgs interactions.

In this work, we extend the theory calculation and implementation of Ref. [12] with the one-loop contributions of top-quark operators to the  $e^+e^- \rightarrow W^+W^-$  process. It allows us to perform a consistent global fit in the SMEFT, with Higgs couplings and TGCs at the tree level and top-quark operators at the one-loop level. Our main focus is on future circular lepton colliders with very good Higgs measurements but not large enough center-of-mass energies to reach the  $t\bar{t}$  or  $t\bar{t}h$  production thresholds. We aim to answer the following questions:

- If future lepton colliders only run below the  $t\bar{t}$  ( $t\bar{t}h$ ) threshold, can they still determine top-quark–gauge-boson (top-quark Yukawa) couplings with high precision?
- Does the uncertainty on top-quark couplings affect the reach of future measurements of Higgs couplings?

The paper is organized as follows. In Section 2, we describe our theory framework. In Section 3, we review the calculation and implementation of Ref. [12], and extend it to include  $e^+e^- \rightarrow W^+W^-$  production. In Section 4, we describe the measurements and the fit. We discuss our results in Section 5 before concluding in Section 6.

## 2 Effective-field-theory framework

In the absence of clear signs of physics beyond the standard model (BSM), a common approach for testing the SM and identifying possible deviations is provided by the SMEFT [20–22]. BSM effects are captured by a series of higher dimensional operators whose coefficients can be related to the parameters of specific models by

a matching calculation. Given that all the operators of odd dimension violate baryon or lepton numbers [23], the most important deviations are expected to be captured by operators of dimension six:

$$\mathcal{L}_{\text{EFT}} = \mathcal{L}_{\text{SM}} + \sum_i \frac{C_i}{\Lambda^2} O_i^{(6)} + \dots \quad (1)$$

Measurements at the LHC and future lepton colliders can be conveniently interpreted in terms of their coefficients.

Two features of the SMEFT are of particular relevance to this work. The first is that theory predictions can be improved systematically, order by order. The SMEFT is a theory that is renormalizable order by order in  $1/\Lambda^2$  [24]. Thus, theory predictions can always be improved to match experimental uncertainties. This is one of the main advantages of the SMEFT over other BSM parametrizations, such as the anomalous coupling approach to top-quark couplings, and the  $\kappa$  framework for Higgs couplings.

The second feature is that the SMEFT gives unambiguous and model-independent results only if all operators up to a given dimension and up to a given loop order are simultaneously included. This motivates the inclusion of top-quark operators at the one-loop level in all Higgs and diboson processes entering our global analysis and not only in loop-induced ones like  $h \rightarrow gg, \gamma\gamma$  or  $Z\gamma$ . In doing so, we include the contribution of each operator considered at its leading order, i.e. at tree level for Higgs operators, and at one-loop level for most top-quark operators. The tree- and loop-level contributions of other operators are not considered. This may be justified either from a bottom-up or from a top-down point of view. Without imposing restrictions on the type of BSM model covered by our SMEFT, one may argue that other operators are sufficiently constrained by measurements different from the ones considered here. One may also argue that the class of models which would dominantly affect the top-quark and Higgs couplings through the operators we consider is worth studying.

Four-fermion operators giving rise to  $e^+e^-t\bar{t}$  contact interactions are also disregarded although they could potentially play a role. They contribute to Higgs and electroweak processes once the top-quark line is closed in a loop. In particular, the two-fermion and the four-fermion operators could not be efficiently discriminated if  $e^+e^- \rightarrow t\bar{t}$  is only measured near threshold [11]. So, without higher energy runs, the Higgs and diboson measurements could potentially be used to break this degeneracy. Therefore, the inclusion of these operators could affect our results. However, these corrections have not been computed so far and would affect the renormalization of other SMEFT operators. The implementation of the one-loop contributions of four-fermion operators as well as a full analysis of their impact are therefore left

to future study. As these four-fermion operators are included in the global tree-level analysis of Ref. [11], we set their coefficients to zero when using results from there.

Our global analysis of Higgs and diboson measurements is based on that of Ref. [5]. Various observables are combined to constrain efficiently all directions of the multidimensional space spanned by the Higgs and top-quark operator coefficients. They will be discussed in Section 4. We work under the same assumptions: departing from flavor universality only to single out top-quark operators and distinguish the various measurable Yukawa couplings, as well as taking electroweak and CP-violating observables perfectly SM-like. We also neglect the quadratic contributions of dimension-six operators as justified in Ref. [5]. Operators that modify Higgs couplings and TGCs are then captured by the following 12 parameters of the Higgs basis:

$$\begin{aligned} \delta c_Z, \quad c_{ZZ}, \quad c_{Z\Box}, \quad \bar{c}_{\gamma\gamma}, \quad \bar{c}_{Z\gamma}, \quad \bar{c}_{gg}, \\ \delta y_t, \quad \delta y_c, \quad \delta y_b, \quad \delta y_\tau, \quad \delta y_\mu, \quad \lambda_Z. \end{aligned} \quad (2)$$

As described in Ref. [5] (with different notations), they can be easily mapped to the coefficients of 12 SILH-like basis operators:

$$\begin{aligned} O_{\varphi W} &= \varphi^\dagger \varphi W_{\mu\nu}^I W^{I\mu\nu}, & O_{\varphi B} &= \varphi^\dagger \varphi B_{\mu\nu} B^{\mu\nu}, \\ O_{\varphi\Box} &= (\varphi^\dagger \varphi) \Box (\varphi^\dagger \varphi), & O_W &= iD^\mu \varphi^\dagger \tau^I D^\nu \varphi W_{\mu\nu}^I, \\ O_B &= iD^\mu \varphi^\dagger D^\nu \varphi B_{\mu\nu}, & O_{b\varphi} &= (\varphi^\dagger \varphi) \bar{Q} b \varphi + h.c., \\ O_{\mu\varphi} &= (\varphi^\dagger \varphi) \bar{l}_2 e_2 \varphi + h.c., & O_{\tau\varphi} &= (\varphi^\dagger \varphi) \bar{l}_3 e_3 \varphi + h.c., \\ O_{t\varphi} &= (\varphi^\dagger \varphi) \bar{Q} t \tilde{\varphi} + h.c., & O_{c\varphi} &= (\varphi^\dagger \varphi) \bar{q}_2 u_2 \tilde{\varphi} + h.c., \\ O_{WW} &= \epsilon^{IJK} W_\mu^I W_\nu^J W_\rho^K, & O_{\varphi G} &= \varphi^\dagger \varphi G_{\mu\nu} G^{\mu\nu}, \end{aligned} \quad (3)$$

where  $Q$  is the third-generation quark doublet. The subscripts 2, 3 are flavor indexes (weak and mass eigenstate fermions are not distinguished, approximating mixing matrixes by the identity). The assumption of perfect electroweak precision measurements in Ref. [5] allowed to disregard the two operators

$$O_{\varphi WB} = \varphi^\dagger \tau^I \varphi W_{\mu\nu}^I B^{\mu\nu}, \quad O_{\varphi D} = (\varphi^\dagger D^\mu \varphi)^* (\varphi^\dagger D_\mu \varphi). \quad (4)$$

In this work, this assumption must be enforced at the one-loop level, including also top-quark operators. This will be discussed in the next section.

The 14 Higgs operators above form a set consistent with the basis employed in the calculation of Ref. [12]. The top-quark operators considered here are the following:

$$\begin{aligned} O_{t\varphi} &= \bar{Q} t \tilde{\varphi} (\varphi^\dagger \varphi) + h.c., \\ O_{\varphi Q}^{(1)} &= (\varphi^\dagger i \overleftrightarrow{D}_\mu \varphi) (\bar{Q} \gamma^\mu Q), \end{aligned}$$

$$\begin{aligned} O_{\varphi Q}^{(3)} &= (\varphi^\dagger i \overleftrightarrow{D}_\mu^I \varphi) (\bar{Q} \gamma^\mu \tau^I Q), \\ O_{\varphi t} &= (\varphi^\dagger i \overleftrightarrow{D}_\mu \varphi) (\bar{t} \gamma^\mu t), \\ O_{tW} &= (\bar{Q} \sigma^{\mu\nu} \tau^I t) \tilde{\varphi} W_{\mu\nu}^I + h.c., \\ O_{tB} &= (\bar{Q} \sigma^{\mu\nu} t) \tilde{\varphi} B_{\mu\nu} + h.c., \\ O_{tG} &= (\bar{Q} \sigma^{\mu\nu} T^A t) \tilde{\varphi} G_{\mu\nu}^A + h.c. \end{aligned} \quad (5)$$

The  $O_{\varphi tb}$  operator is neglected because its interferences with SM amplitudes are suppressed by a factor of  $m_b$ . In addition, we define

$$O_{\varphi Q}^{(+)} \equiv \frac{1}{2} (O_{\varphi Q}^{(1)} + O_{\varphi Q}^{(3)}), \quad O_{\varphi Q}^{(-)} \equiv \frac{1}{2} (O_{\varphi Q}^{(1)} - O_{\varphi Q}^{(3)}), \quad (6)$$

and exclude  $O_{\varphi Q}^{(+)}$  which affects the tightly constrained  $Z \rightarrow b\bar{b}$  branching fraction and asymmetry. Note that  $O_{t\varphi}$  has been included already in the Higgs operators, and its coefficient has a simple relation with  $\delta y_t$ .\*

$$\delta y_t = -\frac{C_{t\varphi} v^2}{\Lambda^2}. \quad (7)$$

In summary, the following 6 top-quark operator coefficients are included in our analysis:

$$C_{\varphi t}, \quad C_{\varphi Q}^{(-)}, \quad C_{tW}, \quad C_{tB}, \quad C_{t\varphi}, \quad C_{tG}. \quad (8)$$

Apart from the top-quark operators, loop corrections also provide new opportunities for indirectly constraining the Higgs trilinear coupling,  $\lambda_3$ . The modification in the this coupling is induced by a dimension-six operator  $O_\varphi = (\varphi^\dagger \varphi)^3$ . The coupling can be directly constrained at the LHC, but only at the  $\mathcal{O}(1)$  level even assuming the high luminosity scenario [25]. It was shown in Ref. [10] that the measurements of the Higgsstrahlung process at lepton colliders can have an indirect but competitive reach on this coupling via its loop contribution. A global analysis was performed in Ref. [8], which showed that the discrimination between the Higgs trilinear coupling and other Higgs operators is possible, but nevertheless nontrivial. In this work, to determine the impact of  $\lambda_3$  on the global reach of the top-quark operators, we follow Ref. [8] and include its one-loop contribution to all the single Higgs processes, parameterized by  $\delta\kappa_\lambda \equiv \kappa_\lambda - 1$ , where  $\kappa_\lambda$  is the ratio of the Higgs trilinear coupling to its SM value,

$$\kappa_\lambda \equiv \frac{\lambda_3}{\lambda_3^{\text{SM}}}, \quad \lambda_3^{\text{SM}} = \frac{m_h^2}{2v^2}. \quad (9)$$

By turning on and off this coupling in our fit, we will see by how much the determination of top-quark couplings will be affected.

\* $\delta y_t$  receives an additional contribution from  $C_{\varphi\Box}$ . It is omitted because  $\delta y_t$  in our calculation enters at the loop level, while we only aim at the LO contribution from  $C_{\varphi\Box}$ .

### 3 Theory predictions

To the precision needed for this work, the theory predictions for, e.g., total cross sections can be written as

$$\sigma = \sigma_{\text{SM}} + C_h(\mu_{\text{EFT}})\sigma_{\text{tree}} + C_t(\mu_{\text{EFT}})\frac{\alpha_{EW}}{\pi}\left(\sigma_{\log}\log\frac{Q^2}{\mu_{\text{EFT}}^2} + \sigma_{\text{fin}}\right). \quad (10)$$

Here,  $C_h(\mu_{\text{EFT}})$  is the coefficient of some Higgs or TGC operator  $O_h$  that contributes at the tree level, and  $\mu_{\text{EFT}}$  is the scale at which the coefficient is defined. In this work we take  $\mu_{\text{EFT}} = m_H$  for all measurements.  $C_t$  is the coefficient of some top-quark operator  $O_t$  which enters at the loop level and could potentially mix into  $O_h$ .  $Q^2$  is the scale of the process. The calculation of  $\sigma_{\text{tree}}$  is straightforward while  $\sigma_{\log}$  can be obtained from the running of SMEFT coefficients. In this section, we review the computation of the genuine electroweak corrections  $\sigma_{\text{fin}}$  carried out in Ref. [12] for Higgs processes. We then compute them for  $e^+e^- \rightarrow W^+W^-$  production.

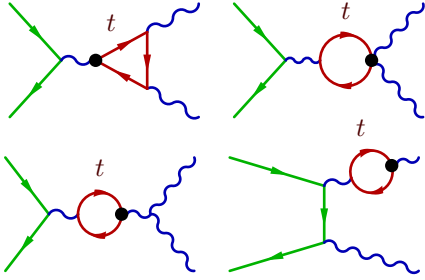


Fig. 1. Selected diagrams for dimension-six top-quark contributions to  $e^+e^- \rightarrow W^+W^-$ . Red lines represent the top quark. Blobs represent dimension-six operator insertions.

The complete set of electroweak NLO corrections from top-quark operators to precision electroweak operators was first given in Ref. [26]. Results can conveniently be obtained in the “star scheme” [27], because all contributions are oblique. For Higgs production this is not any longer the case. In addition to the  $VV$  self-energy corrections one has to compute also  $hh$  and  $hVV$  functions, where  $V$  is a photon,  $W$  or  $Z$  boson. While several calculations were available in the literature [13–19], the complete results for top-quark operator contributions to Higgs production in the  $Vh$  and VBF channels, as well as decay modes  $h \rightarrow \gamma\gamma, \gamma Z, Wl\nu, Zll, b\bar{b}, \mu\mu, \tau\tau$  were first presented in Ref. [12]. This excludes the four-fermion operators mentioned previously. The calculation is implemented in the MadGraph5\_aMC@NLO framework [28] whose reweighting functionality [29] is used to compute the dimension-six top- and bottom-quark loop contributions. The SM parameters are renormalized consistently

in the  $m_W, m_Z$  and  $G_F$  scheme up to dimension six, and operator coefficients are renormalized in the  $\overline{MS}$  scheme. The rational R2 counterterms are computed following the scheme of Ref. [30–32], for  $ZZ, hh, hVV, ffV$  and  $ffh$  loop functions. The implementation provides an automatic and convenient way to simulate indirect contributions from top-quark operators, which enter Higgs processes as NLO electroweak corrections. Events can be generated and matched to parton shower, allowing for detailed investigations using the full differential information.

It is well known that, in the SMEFT formalism, the measurements of Higgs couplings and TGCs are entangled [33–35].  $W$  pair production is therefore an important component of global Higgs analyses at future lepton colliders. For this reason, we extend the calculation of Ref. [12] to incorporate the  $e^+e^- \rightarrow W^+W^-$  process. Some diagrams involving dimension-six operators are shown in Fig. 1. Additional counterterms need to be computed for the  $WW\gamma$  and  $WWZ$  vertexes. Among the three TGC operators, only  $O_W$  and  $O_B$  are renormalized by top-quark operators. The anomalous dimensions are derived in Ref. [12]. Another difficulty is that the  $WW\gamma$  function involves a triangle anomaly diagram. In our scheme, this implies that the R2 counterterms depend on the choice of the vertex from which the trace of the fermion loop starts. This effect is in principle canceled by a Wess-Zumino term generated when chiral fermions in the full theory are integrated out [36]. The problem can be fixed by imposing the Ward identity of the photon in the low-energy effective theory. We provide more details in Appendix A. We have validated our implementation of the  $WW\gamma$  vertex by computing processes with an external photon and checking that the Ward identity is satisfied.

Our global analysis relies on the assumption that precision electroweak measurements are perfectly constrained to be SM-like. This has consequences on our renormalization scheme, as explained in the following.

In our operator basis, precision electroweak observables receive tree-level contributions from  $O_{\varphi WB}$  and  $O_{\varphi D}$  operators. At that order, their coefficients are thus simply removed from the fit by assuming the measurements of precision electroweak observables perfectly match SM predictions. Top-quark operators however start contributing at the loop level. In the  $\overline{MS}$  scheme, the same assumption implies that  $C_{\varphi WB}$  and  $C_{\varphi D}$  need to take specific values to cancel these loop corrections. These nonzero values will then in turn modify other Higgs production and decay channels, making the fit more complicated. In Ref. [12], a more convenient approach has been followed, where  $C_{\varphi WB}$  and  $C_{\varphi D}$  are defined in the on-shell scheme using oblique parameters as renormalization conditions. Therefore, if the oblique pa-

rameters are tightly constrained, we can exclude  $C_{\varphi WB}$  and  $C_{\varphi D}$  from the fit.

Instead of using oblique parameters, we further refine this approach in this work, by using the full set of  $Z$ -pole and  $W$ -pole measurements listed in Ref. [37] as our renormalization conditions. We assume that, apart from deviations in the top-quark and the Yukawa sectors, BSM effects are otherwise universal, in the sense that they can be captured by dimension-six operators which involve SM bosons only, up to suitable field redefinitions [38]. Their effects in Higgs,  $WW$ , and  $Z/W$ -pole measurements are then fully captured by operators listed

$$\alpha \rightarrow \alpha_* = \alpha + \delta\alpha = \alpha \left( 1 - \Pi'_{\gamma\gamma}(q^2) + \Pi'_{\gamma\gamma}(0) \right) \times \left[ 1 - \frac{d}{dq^2} \Pi_{ZZ}(q^2) \Big|_{q^2=m_Z^2} + \Pi'_{\gamma\gamma}(q^2) + \frac{c_W^2 - s_W^2}{s_W c_W} \Pi'_{\gamma Z}(q^2) \right], \quad (11)$$

$$m_Z^2 \rightarrow m_{Z*}^2 = m_Z^2 + \delta m_Z^2 = m_Z^2 + \Pi_{ZZ}(m_Z^2) - \Pi_{ZZ}(q^2) + (q^2 - m_Z^2) \frac{d}{dq^2} \Pi_{ZZ}(q^2) \Big|_{q^2=m_Z^2}, \quad (12)$$

$$s_W^2 \rightarrow s_{W*}^2 = s_W^2 + \delta s_W^2 = s_W^2 \left[ 1 + \frac{c_W}{s_W} \Pi'_{\gamma Z}(q^2) + \frac{c_W^2}{c_W^2 - s_W^2} \left( \Pi'_{\gamma\gamma}(0) + \frac{1}{m_W^2} \Pi_{WW}(0) - \frac{1}{m_Z^2} \Pi_{ZZ}(m_Z^2) \right) \right]. \quad (13)$$

and taking  $q^2 = m_Z^2$ . Here  $\Pi_{VV}(q^2)$  is the self-energy correction for the  $V = \gamma, W, Z$  gauge boson while  $\Pi'_{VV}(q^2) \equiv [\Pi_{VV}(q^2) - \Pi_{VV}(0)]/q^2$ . Expressions for these corrections are of order  $C/\Lambda^2$  and can be found in Ref. [26]. Note that unlike in the calculation for Higgs and  $WW$  production, here we use  $G_F$  instead of  $m_W$  as an input parameter, since theory predictions in Ref. [37] are provided in this scheme.

$Z$ -pole observables consist of various combinations of partial widths and asymmetries. Their SM predictions only depend on  $s_W$  and on the product of  $\alpha$  and  $m_Z$ . Thus these measurements only constrain two independent combinations of top-quark operator coefficients. The correction to the  $W$  mass can be written as

$$\begin{aligned} \frac{\delta m_W^2}{m_W^2} &= \frac{s_W^2}{c_W^2 - s_W^2} \Pi'_{\gamma\gamma}(0) + \frac{c_W^2}{c_W^2 - s_W^2} \frac{1}{m_W^2} \Pi_{WW}(0) \\ &\quad - \frac{c_W^2}{c_W^2 - s_W^2} \frac{1}{m_Z^2} \Pi_{ZZ}(m_Z^2) + \Pi'_{WW}(m_W^2). \end{aligned} \quad (14)$$

and constitutes the third independent combination constrained. Finally, the width of the  $W$  boson is corrected by

$$\begin{aligned} \delta \left( \frac{\Gamma_W}{m_W} \right)^2 &= \left( \frac{\Gamma_W}{m_W} \right)^2 \times \\ &\quad \left( \frac{\delta m_W^2}{m_W^2} - \Pi'_{WW}(m_W^2) + \frac{d}{dq^2} \Pi_{WW}(q^2) \Big|_{q^2=m_W^2} \right) \end{aligned} \quad (15)$$

which is almost degenerate with the previous constraint. Given the relatively weaker precision on the measure-

ment of  $\Gamma_W$  and the approximate degeneracy, we expect this fourth constraint to be less useful.

We now modify the renormalization of  $C_{\varphi WB}$  and  $C_{\varphi D}$  by finite  $\Delta_{ij}$  constants, so that

$$C_i \Rightarrow Z_{ij} C_j = C_i + \delta Z_{ij} C_j, \quad (16)$$

$$\delta Z_{ij} = \frac{\alpha}{2\pi} \Gamma(1+\epsilon) \left( \frac{4\pi\mu^2}{\mu_{\text{EFT}}^2} \right)^\epsilon \left( \frac{1}{\epsilon} + \Delta_{ij} \right) \gamma_{ij} \quad (17)$$

for  $O_i = O_{\varphi WB}, O_{\varphi D}$ . The  $O_j$  cover all top-quark operators. We then need to choose the values of  $\Delta_{ij}$  which minimize the deviations in the precision observables when setting  $C_{\varphi WB} = C_{\varphi D} = 0$ . To find them, we construct a  $\chi^2$  using the experimental results and theory predictions for all  $W$  and  $Z$  pole data listed in Ref. [37]. The associated covariance matrix has four positive eigenvalues, corresponding to the four independent constraints expected. The  $\Delta_{ij}$  are chosen such that the two most constrained eigenvectors only involve  $C_{\varphi WB}$  and  $C_{\varphi D}$ :

$$+0.906 C_{\varphi WB} + 0.423 C_{\varphi D} = 0 \pm 0.0000234 \quad (18)$$

$$-0.423 C_{\varphi WB} + 0.906 C_{\varphi D} = 0 \pm 0.0124 \quad (19)$$

for  $\Lambda = 1$  TeV. In this specific scheme and up to one-loop order, the two most stringent limits from  $Z$ - and  $W$ -pole data only constrain the renormalized  $C_{\varphi WB}$  and  $C_{\varphi D}$  to small values. The assumption of perfect precision measurements approximates these two limits to be infinitely constraining and allows us to exclude  $C_{\varphi WB}$  and  $C_{\varphi D}$

<sup>†</sup>In the SILH basis, two additional operators  $O_{2B} = -\frac{1}{2}(\partial^\mu B_{\mu\nu})^2$  and  $O_{2W} = -\frac{1}{2}(D^\mu W_{\mu\nu}^a)^2$  are universal, but they can be eliminated in favor of four-fermion operators, and thus drop out from the pole measurements.

from the rest of our analysis at the one-loop level. This can be interpreted as using the first two degrees of freedom of the precision measurements as on-shell renormalization conditions for these two coefficients.

There are two remaining constraints. One is associated with a covariance matrix eigenvalue of about  $300 \text{ TeV}^{-2}$ , is the weakest. We therefore ignore it. The other implies  $0.17C_{\varphi Q}^{(-)} - 0.10C_{\varphi t} - 0.04C_{tB} - 0.92C_{tW} = 0 \pm 0.60 \times (\Lambda/\text{TeV})^2$  and involves only top-quark operators. We include this constraint in our fit, conservatively assuming that it could be strengthened by a factor of five with future lepton collider data. Our final results are however largely insensitive to this constraint.

The above renormalization scheme as well as the  $W$ -pair process are then supplemented to the UFO model described in Ref. [12]. It allows for the automatic calculations of all Higgs and  $W$ -pair processes relevant to this work. Beside inclusive cross sections, differential distributions can also be obtained. The production angle in  $e^+e^- \rightarrow W^+W^-$  will be used in our analysis.

Our discussion so far excluded the top-quark chromodipole operator  $O_{tG}$ . It enters  $h \rightarrow gg$  through a top-quark loop which has already been studied in the literature [39, 40]. This effect will be included in our global analysis.

## 4 Measurements and fit

In this section, we describe the measurements and observables used in our analysis. Since our study is most relevant for lepton colliders with very good Higgs measurements but not large enough center-of-mass energies to reach the  $t\bar{t}$  or  $t\bar{t}h$  production thresholds, our primary focus will be on the circular colliders. Currently, two proposals for such colliders have been made: the Circular Electron Positron Collider (CEPC) in China [41], and the Future Circular Collider with  $e^+e^-$  beams (FCC-ee) at CERN [42]. In this study, we consider the following hypothetical scenario: a circular collider (CC) collecting an integrated luminosity of  $5 \text{ ab}^{-1}$  at a center-of-mass energy of 240 GeV and possibly also running at the top-quark pair production threshold with  $0.2 \text{ ab}^{-1}$  gathered at 350 GeV and  $1.5 \text{ ab}^{-1}$  at 365 GeV. The incoming electron and positron beams are assumed to be unpolarized. This scenario follows closely the current projected run plan of the FCC-ee [43]. The 350 and 365 GeV runs could fix the top-quark electroweak couplings by directly probing  $t\bar{t}$  production, though approximate degeneracies would remain due to limited energy lever arm. The top-quark Yukawa coupling, on the other hand, cannot be directly probed in such a run scenario. We will also show results with only a 240 GeV run, which represents the CEPC scenario. At the moment, there is no plan for the CEPC to run at center-of-mass energies

beyond 240 GeV, though a future upgrade to the top-quark pair production threshold remains an open possibility. Our study could then provide useful information regarding the impact of a 350 GeV upgrade on the measurements of the top-quark couplings and on the indirect effect of their loop contributions on Higgs coupling determinations. Both CEPC and FCC-ee plan to also run at the  $Z$ -pole and  $WW$  production threshold, which could significantly improve the sensitivities on the electroweak observables that are already tightly constrained by LEP measurements.

Linear colliders, such as the Compact Linear Collider at CERN [44] and the International Linear Collider [45], could run at higher energies and, in particular, above the thresholds for both  $t\bar{t}$  and  $t\bar{t}h$  productions. With these measurements, the top-quark operators can be probed at the tree level, with a sensitivity far better than the current one. Although information about top-quark couplings may only be indirectly available at the first 250 GeV stage of the ILC, we will not treat this case explicitly and will not further consider linear collider scenarios.

Table 1. Estimates for the precision reachable on key top-quark observables at the HL-LHC.

Channels	Uncertainties	
	without th. unc.	with th. unc.
$t\bar{t}$	4% [46]	7%
Single top ( $t$ -ch.)	4% [47]	4%
$W$ -helicity ( $F_0$ )	3% [48]	3%
$W$ -helicity ( $F_L$ )	5% [48]	5%
$t\bar{t}Z$	10%	15%
$t\bar{t}\gamma$	10%	17%
$t\bar{t}h$	10%	16% [49]
$gg \rightarrow h$	4%	11% [49]

The HL-LHC measurements could provide important complementary information. To the best of our knowledge, a systematic determination of the projected sensitivity to top-quark couplings is unfortunately not available in the literature. We therefore consider the measurements in Table 1 and estimate the precision reachable with the HL-LHC. Here, the projected precisions on measurements of the  $t\bar{t}$  and  $t$ -channel single top-quark production cross sections and  $W$ -helicity in top-quark decay are based on the works referred to. Theoretical uncertainties for single top-quark production and  $W$ -helicity measurements are neglected, as they are both of order  $\mathcal{O}(1\%)$  [50, 51]. The uncertainties on  $t\bar{t}h$  and  $gg \rightarrow h$  production cross sections are taken from Ref. [49]. The ones imposed on the  $t\bar{t}Z/\gamma$  cross sections are simple estimates. Theoretical uncertainties are estimated from predictions at NLO in QCD. A combination of  $t\bar{t}$ ,  $t\bar{t}h$  and  $gg \rightarrow h$

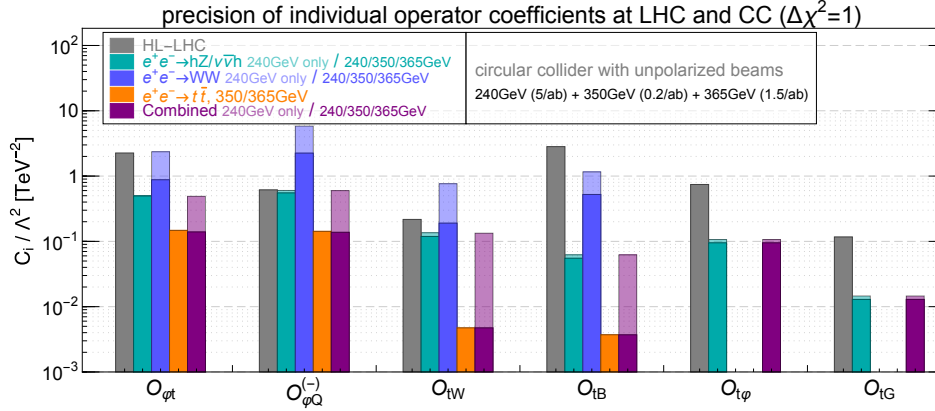


Fig. 2. Individual one-sigma reach on top-quark operator coefficients for different future collider scenarios and measurements. One single coefficient is allowed to depart from zero at a time.

production cross section measurements is sufficient to constrain  $O_{tG}$ ,  $O_{t\varphi}$  and  $O_{\varphi G}$  ( $\bar{c}_{gg}$ ). The  $W$ -helicity measurements alone fix  $O_{tW}$ . The remaining three operators,  $O_{\varphi t}$ ,  $O_{\varphi Q}^{(-)}$  and  $O_{tB}$  are constrained by  $t\bar{t}Z/\gamma$  and single top-quark production cross section measurements. For the trilinear Higgs self-coupling, we follow Ref. [52, 53] and assume that a constraint of  $-0.9 < \delta\kappa_\lambda < 1.3$  at the  $\Delta\chi^2 = 1$  level could be obtained at the HL-LHC by measuring both the rate and the distributions of the double Higgs production process. While a global fit should in principle be performed also for the HL-LHC, it was shown in Ref. [52] that the reach on the trilinear Higgs coupling is dominated by the measurement of the double Higgs production, while the other Higgs operators are well constrained by the single Higgs processes and have little impact on the extraction of the trilinear Higgs coupling. We expect this to hold even with the inclusion of top-quark operator contributions in the loops. The combination of measurements in Table 1 with that of double Higgs production captures the most important information on top-quark operators and the trilinear Higgs self-coupling at the HL-LHC.

For the Higgs measurements at lepton colliders, we follow closely the treatment of Ref. [5] and include both the inclusive  $e^+e^- \rightarrow hZ$  cross section and exclusive Higgs decay channels, as well as the measurement of the  $WW$ -fusion production channel,  $e^+e^- \rightarrow \nu\bar{\nu}h$ . The run scenario in Ref. [5] has been updated to the one detailed above. While the differential observables in  $e^+e^- \rightarrow hZ$  could provide additional information [54, 55], they are not included in our analysis. For these observables, corrections in production and decay of the Higgs and  $Z$  need to be simulated simultaneously, and this is not yet possible in our setup. For the diboson production process,  $e^+e^- \rightarrow W^+W^-$ , we consider only the semileptonic decay channel, assuming the statistical uncertainties dominate. In contrast with Ref. [5], we only include the differential distributions of the  $W$ -production polar angle.

Finally, for the measurements of  $t\bar{t}$  production at center-of-mass energies of 350 and 365 GeV, we use the results of Ref. [11]. We do not consider the one-loop corrections to  $e^+e^- \rightarrow t\bar{t}$  from the top-quark operators, since most of them enter at tree level and can therefore be tightly constrained. In particular, the loop-level dependence in the top-quark Yukawa and chromo-dipole operators are not accounted for. The total  $\chi^2$  is obtained by summing over the  $\chi^2$  of all the measurements whose central values are assumed to confirm SM predictions.

It was shown in Ref. [5] that, thanks to the high precision of the measurements at the lepton colliders, it is sufficient to only keep the linear dependences of the observables on the EFT parameters. We found this statement to hold even with the inclusion of the top-quark operator in loops. However, at the HL-LHC, the cross section for  $t\bar{t}$  production in association with a  $Z$  boson or photon has a limited sensitivity to the linear contributions of  $O_{tW}$  and  $O_{tB}$  [56], due to the Lorentz structure of these dipole operators and to accidental cancellations between different initial states. The inclusion of the  $W$ -helicity measurement significantly improves the reach on  $O_{tW}$  and brings its dependence in the fit back to the linear regime. For  $O_{tB}$ , on the other hand, the reach is much worse and is mainly driven by the quadratic terms. The inclusion of these terms would significantly complicate our fitting procedure. Since our focus is rather on the lepton colliders, we simplify the fit by keeping only the linear terms while adding by hand an extra term to the total  $\chi^2$  that corresponds to a standard deviation of  $3 \text{ TeV}^{-2}$  for  $C_{tB}/\Lambda^2$ , which reproduces the main constraints on  $O_{tB}$  from the square contributions to a good approximation.

## 5 Results

In this section, we present the precision reach obtained by a  $\chi^2$  fit to the observables described in the

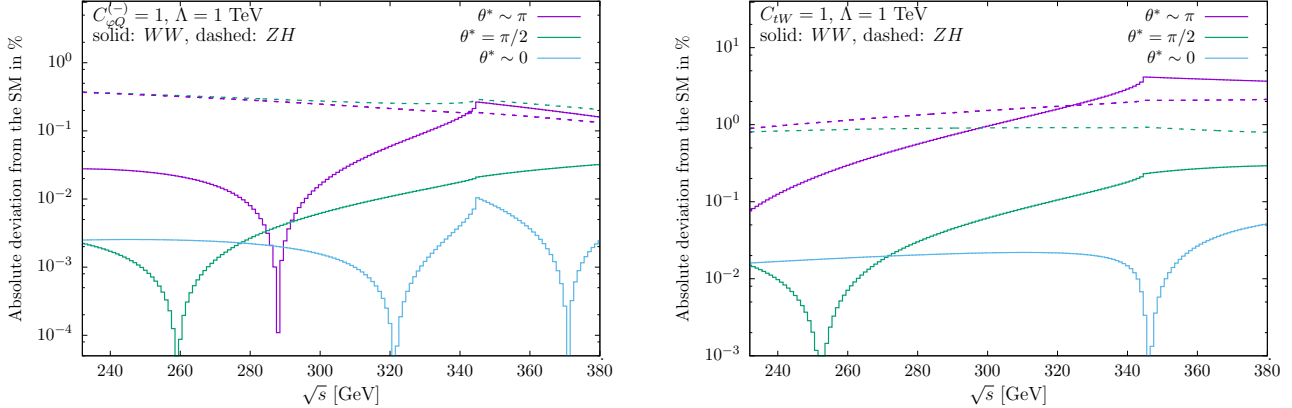


Fig. 3. Center-of-mass energy dependence of  $O_{\varphi Q}^{(-)}$  (left) and  $O_{tW}$  (right) contributions to  $e^+e^- \rightarrow W^+W^-$  (solid) and  $Zh$  (dashed) production in percent of the SM rate, for  $C/\Lambda^2 = 1$  TeV $^{-2}$ . Dependences are shown in absolute values (changes of sign generate the visible dips) for three different scattering angles: 0,  $\pi/2$  and  $\pi$ . For  $e^+e^- \rightarrow Zh$ , the 0 and  $\pi$  curves overlap.

previous section. There are two important aspects in the determination of the indirect reach on the top-quark operators from the Higgs and diboson measurements at lepton colliders. First, the overall measurement sensitivity is assessed by performing individual fits to each parameter of Eq. (8), setting all others to zero. The second aspect concerns the discrimination among top-quark operators, and between the Higgs and top-quark ones. Differential information is then crucial to constrain all directions of the SMEFT parameter space with a limited number of processes. Runs at different center-of-mass energies and with different polarizations also help setting meaningful constraints with lepton collider data only, though the latter information is not available at circular colliders. One can otherwise also resort to a combination with HL-LHC measurements.

The individual sensitivities to the top-quark operators of Eq. (8) are shown in Fig. 2 for different measurements at a circular lepton collider as well as at the HL-LHC. The results are presented in terms of the one-sigma reach on  $C_i/\Lambda^2$ , with  $C_i$  and  $\Lambda$  defined in Eq. (1). Five scenarios are considered. The first column corresponds to the HL-LHC measurements listed in Table 1, with theoretical uncertainties included. The second, third and fourth columns respectively include the Higgs, diboson, and  $t\bar{t}$  measurements at a circular lepton collider. The last column is obtained from the combination of all these circular collider measurements. Lighter shades are obtained with a 240 GeV run only, while the darker ones combine operation all three center-of-mass energies considered (240, 350 and 365 GeV).

The indirect individual reach of Higgs and diboson measurements at 240 GeV on top-quark operator coefficients is seen to be better than the direct HL-LHC sensitivity. The loop suppression of top-quark operator contributions is compensated by the high precision of lepton

colliders measurements. This is one of the main conclusions of this work, and partly answers the first question raised in the introduction. If higher center-of-mass energies are available, direct  $e^+e^- \rightarrow t\bar{t}$  measurements still provide the best reach on top-quark operators. Note that the tree-level analysis of the top-quark pair production from Ref. [11] is insensitive to the top-quark Yukawa and chromo-dipole operators. The indirect individual reach of the diboson measurements at 240 GeV is somewhat lower than that of Higgs measurements. It however improves with 350/365 GeV runs. This higher indirect sensitivity of  $W$  pair production to top-quark operators at higher center-of-mass energies is further examined in Fig. 3. For illustration, the contributions of  $O_{\varphi Q}^{(-)}$  and  $O_{tW}$  operators are shown in percent of the SM rate, as a function of the center-of-mass energy and for three scattering angles. For comparison, dashed curves show the dependence of  $e^+e^- \rightarrow Zh$  production.

Among top-quark operators, the improvement brought by 240 GeV Higgs measurements over HL-LHC individual sensitivities is most significant for  $O_{tB}$ . It mainly arises from the measurement of the Higgs decay to two photons,  $h \rightarrow \gamma\gamma$ . As shown in Ref. [12], the  $O_{tB}$  operator has a particularly large contribution to this decay channel: roughly of the same size as the SM rate when  $C_{tB}/\Lambda^2 = (1 \text{ TeV})^{-2}$ . On the other hand, no direct measurements at the LHC can probe  $O_{tB}$  efficiently. It should be noted that the measurements of  $h \rightarrow \gamma\gamma$  at the HL-LHC could also help probing  $O_{tB}$ . Similarly,  $O_{t\varphi}$  and  $O_{tG}$  can be very well constrained individually by the measurement of  $h \rightarrow gg$  at lepton colliders. However, we will see in our global analysis that the degeneracy between the top-quark and Higgs operators is to be partially lifted by loop corrections in other Higgs processes.

In Fig. 4, we present the results of the global analysis for all Higgs and top-quark operator coefficients of

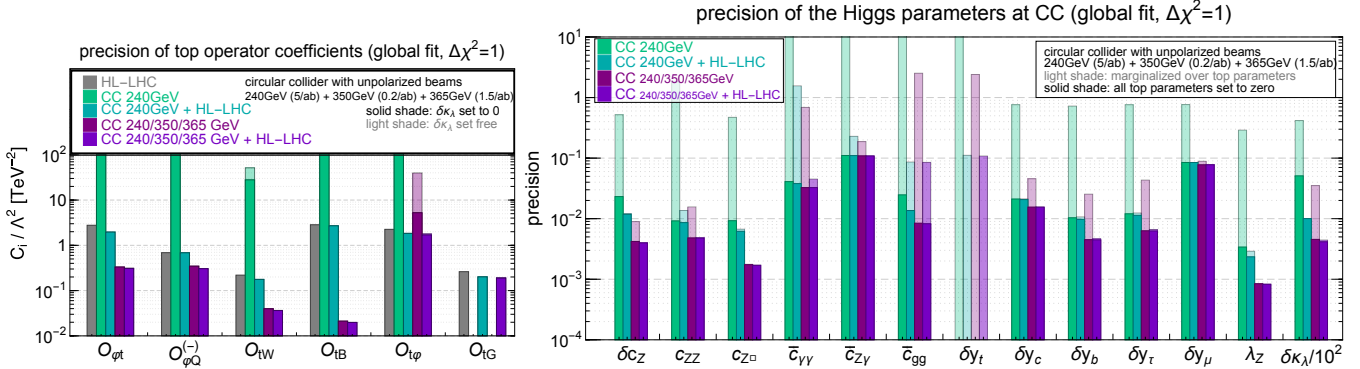


Fig. 4. Global one-sigma precision reach on the 18 top-quark (left) and Higgs (right) operator coefficients deriving from HL-LHC and circular lepton collider measurements. The Higgs parameter definitions are that of Ref. [5]. Large degeneracies are present in the CC 240 GeV scenario and push the precision reach on some operator coefficients outside of the plot range. With lepton-collider measurements only,  $C_{tG}$  and  $\bar{c}_{gg}$  remain fully correlated. The constraint displayed for  $\bar{c}_{gg}$  is then actually to be interpreted as applying on  $\bar{c}_{gg} + 0.46 C_{tG}$ .

Eq. (2) and (8). It amounts to 18 degrees of freedom once the trilinear Higgs boson self-coupling is included. Note that  $\delta y_t$  and  $C_{t\varphi}$  represent the same degree of freedom since they are related through Eq. (7). The reach on the top-quark and Higgs operator coefficients is respectively shown in the left and right panels. For top-quark operators, five scenarios are presented. The first column shows the reach of the HL-LHC measurements. The second column shows the indirect reach of a 240 GeV run. This result is then combined with the HL-LHC measurements and displayed in the third column. The fourth and the fifth columns display similar information, but with all three energies, 240, 350 and 365 GeV. The  $e^+e^- \rightarrow t\bar{t}$  measurements are then in particular included. We also display the impact of  $\delta\kappa_\lambda$  on the reach of the top-quark operators. The results shown with the light shades are obtained by setting  $\delta\kappa_\lambda$  to zero, and the ones with darker shades are obtained by marginalizing over  $\delta\kappa_\lambda$ . The impact of  $\delta\kappa_\lambda$  is small once the double Higgs measurements of the HL-LHC are included.

As expected, the indirect global reach of Higgs and diboson measurements on top-quark operator coefficients is much lower than the individual one. In particular, large degeneracies are present when data from a 240 GeV run only is exploited, pushing global limits beyond the range of validity of the EFT. While the dependence of observables used in the fit on dimension-six operator coefficients is still dominated by linear contributions, these limits should be interpreted with care. The difference between individual and global constraints is particularly pronounced for  $C_{tB}$ ,  $C_{t\varphi}$  and  $C_{tG}$  due to their approximate degeneracies with Higgs operators. The  $h \rightarrow \gamma\gamma$  branching fraction is for instance very well constrained but, alone, does not discriminate between the contributions from  $C_{t\varphi}$ ,  $C_{tB}$  and  $\bar{c}_{\gamma\gamma}$ . Similarly,  $h \rightarrow gg$  measure-

ments only constrain a combination of  $C_{t\varphi}$ ,  $C_{tG}$  and  $\bar{c}_{gg}$ . Lepton collider runs nevertheless provide some marginal improvement in a combination with direct top-quark measurements at the HL-LHC. Note that the  $O_{tG}$  operator enters  $h \rightarrow gg$  but no other measurement at 240 GeV. So its marginalized limit without combination with HL-LHC data is absent. At higher energies, it could enter in NLO corrections to  $t\bar{t}$  production (or in  $t\bar{t}j$ ) which we do not include. This is in contrast with  $O_{t\varphi}$  whose marginalized limit at lepton colliders derive from its loop corrections to other channels which are however not loop-induced. We will further discuss the reach on the top-quark Yukawa coupling at the end of this section. Direct measurements of  $e^+e^- \rightarrow t\bar{t}$  still yield the best handle on top-quark operator coefficients. As mentioned earlier, it remains to be examined whether they are also efficient in constraining indirectly the  $O_{t\varphi}$  and  $O_{tG}$  operator coefficients in a global analysis. In our treatment, the main constraints on these parameters arise from the HL-LHC measurements of  $t\bar{t}$ ,  $t\bar{t}h$ , and  $gg \rightarrow h$ .

In the right panel of Fig. 4, the one-sigma reach on Higgs couplings are presented for circular lepton colliders with and without combination with HL-LHC data. The impact of a 240 GeV run alone is again separated from that of the full scenario considered, with operation at center-of-mass energies of 240, 350 and 365 GeV. In this figure, we aim to answer the second question raised in the introduction, by emphasizing the impact of uncertainties on top-quark couplings on the extraction of Higgs couplings. This is visible in the difference between bars of lighter and darker shades, for which the corresponding top-quark operator coefficients (including  $\delta y_t$ ) are respectively marginalized over or set to zero. Considering a lepton collider run at 240 GeV only, without any direct constraint on top-quark operator coefficients, these

uncertainties typically worsen the reach on most Higgs couplings by more than one order of magnitude. Several global limits — on  $\bar{c}_{\gamma\gamma}$ ,  $\bar{c}_{Z\gamma}$  and  $\bar{c}_{gg}$  in particular — are then too loose to remain meaningful. The impact of the top-quark loop contributions on most Higgs couplings is significantly reduced once direct top-quark pair production measurements are performed above the  $e^+e^- \rightarrow t\bar{t}$  production threshold. The uncertainty on the top-quark Yukawa coupling still sizeably affects the determination of several Higgs boson couplings. The HL-LHC data cures this issue for all couplings but  $\bar{c}_{gg}$ . Without lepton collider run above the  $t\bar{t}$  production threshold, the loose constraint on  $C_{tB}$  deriving from HL-LHC measurements degrades the global limit on  $\bar{c}_{\gamma\gamma}$  by more than one order of magnitude.

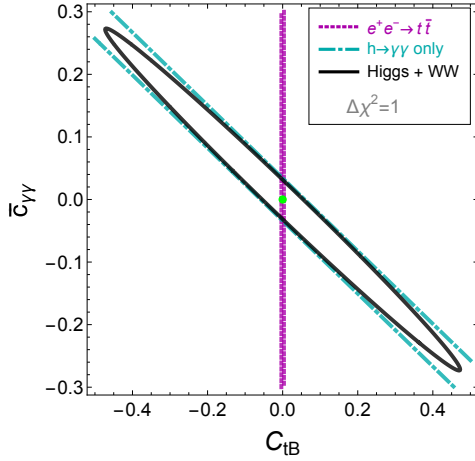


Fig. 5. Two-dimensional constraints on  $C_{tB}$  and  $\bar{c}_{\gamma\gamma}$ , with all other parameters set to zero, to illustrate the correlation between Higgs and top-quark couplings.

This correlation is further examined in Fig. 5 showing the individual  $\Delta\chi^2 = 1$  sensitivities of various measurements in the two-dimensional parameter space formed by  $C_{tB}$  and  $\bar{c}_{\gamma\gamma}$ . The  $h \rightarrow \gamma\gamma$  measurement imposes a tight constraint on a linear combination of  $C_{tB}$  and  $\bar{c}_{\gamma\gamma}$ , leading to a strong correlation between these two parameters, but also leaving a blind direction unconstrained. The latter can be lifted either at lepton collider via loop corrections involving  $O_{tB}$  to other processes, or at the HL-LHC via direct  $t\bar{t}Z/\gamma$  measurements, but none of them is strong enough to simultaneously pin down both couplings. In particular, HL-LHC measurements yield a loose  $-2.7 < C_{tB} < 2.1$  constraint for  $\Lambda = 1$  TeV which cannot be displayed in Fig. 5. As already stressed, direct  $e^+e^- \rightarrow t\bar{t}$  measurements above 350 GeV are needed to resolve this issue. Similar observations can also be made for  $\bar{c}_{Z\gamma}$ . The lower precision achieved on the  $hZ\gamma$

interaction somewhat reduces the impact of correlations in that case.

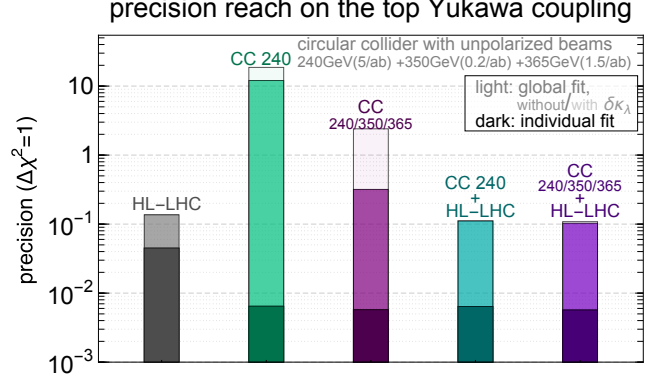


Fig. 6. Indirect one-sigma reach on  $\delta y_t$  in different lepton collider scenarios, compared and combined with the HL-LHC measurements.

Finally, we show in Fig. 6 the indirect reach on the top-quark Yukawa coupling,  $\delta y_t$ , from Higgs and diboson measurements at a circular lepton collider. With only a 240 GeV run at a circular lepton collider, a strong correlation with  $\bar{c}_{gg}$  makes the global reach on  $\delta y_t$  about three orders of magnitude weaker than the individual one. The individual reach is dominated by the precision of the  $h \rightarrow gg$  branching fraction measurement (see also Ref. [57]). In contrast, the global one is determined by loop-level sensitivity of processes that are not loop-induced. Additional runs at center-of-mass energies of 350 and 365 GeV directly fix top-quark–gauge-boson couplings through  $e^+e^- \rightarrow t\bar{t}$  measurements and improve the global constraint on  $\delta y_t$  by more than an order of magnitude. Still, an approximate degeneracy with the loop-dependence on the trilinear Higgs self-coupling is visible and is only resolved by a combination with HL-LHC measurements.<sup>‡</sup> The loop-level sensitivity of  $e^+e^- \rightarrow t\bar{t}$  on  $\delta y_t$  which we did not include is potentially complementary. With a CLIC beam spectrum (broader than that of a circular collider), a  $t\bar{t}$  threshold scan alone leads to a precision of about 20% on  $\delta y_t$  determined simultaneously with the top-quark mass using a total integrated luminosity of  $100 \text{ fb}^{-1}$  [59]. Setting  $\delta\kappa_\lambda$  to zero, the indirect sensitivity of Higgs and diboson processes in runs at center-of-mass energies of 240, 350 and 365 GeV leads to a global one-sigma precision of 32% on  $\delta y_t$ . This reach is competitive with the one achievable at the HL-LHC. To compare with direct measurements, the  $e^-e^+ \rightarrow t\bar{t}h$  production cross section with  $1 \text{ ab}^{-1}$  of integrated luminosity collected at a center-of-mass energy of 500 GeV with a  $P(e^+, e^-) = (+0.3, -0.8)$  beam

<sup>‡</sup>Conversely, the impact of the uncertainty on  $\delta y_t$  in the extraction of  $\delta\kappa_\lambda$  through loop corrections in  $e^+e^- \rightarrow hZ$  at 240 GeV was studied in Ref. [58].

polarization would lead to a precision of 10% on  $\delta y_t$  [60]. We thus conclude that the loop contributions to Higgs and diboson processes studied in this work provide an additional handle on  $\delta y_t$  below the  $t\bar{t}h$  threshold, leading a global reach competitive with that of other direct and/or indirect approaches. This completes the answer to the first question in our introduction.

## 6 Conclusions

In this work, we have studied the sensitivity of a future circular  $e^+e^-$  collider to Higgs couplings, triple gauge-boson couplings, and top-quark couplings. In particular, we focused on runs below the  $e^+e^- \rightarrow t\bar{t}$  production threshold, where top-quark couplings enter as one-loop corrections. The corrections to the Higgs processes became available in Ref. [12]. We have obtained the corrections to  $W$ -boson pair production which were not previously known. Based on these results, we have performed a global SMEFT analysis including both Higgs and  $W$ -pair measurements. This allowed us to derive the future sensitivities to all couplings considered simultaneously.

The main finding of this work is that future lepton colliders running at center-of-mass energies below the  $t\bar{t}$  threshold can provide useful information on top-quark couplings through the measurements of virtual effects. The indirect individual sensitivities obtained are higher than the direct HL-LHC ones. Nevertheless, our analysis suggests that an energy upgrade above the  $e^+e^- \rightarrow t\bar{t}$  production threshold is desirable. On the one hand, the direct individual sensitivity to top-quark couplings is much higher. On the other hand, the strong correlations between the top-quark and Higgs couplings which manifest themselves in a global analysis are mitigated. Below the  $t\bar{t}$  threshold, global constraints on top-quark couplings are otherwise much weaker than individual ones, **if meaningful at all**. The combination a 240 GeV run with direct top-quark coupling measurements at the HL-LHC does not entirely solve this issue. A precise determination of top-quark couplings is thus also crucial for fixing Higgs couplings.

In addition, we find that lepton colliders running below the  $t\bar{t}h$  production threshold can also determine the top-quark Yukawa coupling through its loop corrections to other Higgs channels. Combining 240 GeV and 350/365 GeV runs leads to a marginalized limit that is competitive with projected direct limits at the HL-LHC as well as at the ILC with 500 GeV of center-of-mass energy. Higgs and diboson measurements thus provide an alternative indirect determination of the top-quark Yukawa coupling at future circular lepton collider, beside a  $t\bar{t}$  threshold scan. Given that latter is also affected by the mass of the top quark and the former by loops

of the trilinear Higgs self-coupling, the two approach are expected to be complementary. This interplay should be further studied in the future. Note that the 350/365 GeV runs are crucial for the precision of this approach. This provides another motivation for the corresponding energy upgrade at circular lepton colliders.

A few simplifications have been made throughout our analysis. Four-fermion and CP-odd operators were not included, as the corresponding electroweak NLO corrections are yet not available. Top-quark pair production at lepton colliders was treated at tree level. Precision electroweak measurements were assumed to be infinitely constraining. Our approach could be applied to the lower-energy stages of a linear collider where beam polarization would provide an additional handle. A more extensive use of differential distributions could also improve the reach we presented here and help lifting approximate degeneracies. Further investigations along these directions can be envisioned.

## Acknowledgements

We thank C. Grojean and M. Riemann for helpful discussions about the fit, X. Zhao for useful discussions about renormalization schemes, and Y. Bai and K. Mimasu for useful discussions about chiral anomaly in the SMEFT. CZ is supported by IHEP under Contract No. Y7515540U1. EV is supported by a Marie Skłodowska-Curie Individual Fellowship of the European Commission's Horizon 2020 Programme under contract number 704187.

## A Gauge anomaly in the $WW\gamma$ vertex

Effective operators could induce gauge anomalies by modifying the top-quark couplings to gauge bosons, which are chiral. In our scheme, this is reflected by the fact that the R2 rational counterterms of the  $W^+W^-\gamma$  loop function contain a term with the epsilon tensor, whose coefficient depends on the vertex from which we compute the fermionic trace. In the following, we list the epsilon term in the R2 counterterms for all relevant operators, with the fermion loop traced from all three vertexes,  $\gamma$ ,  $W^+$ , and  $W^-$ . Our convention is that the three external fields,  $A^\mu$ ,  $W^{+\nu}$ , and  $W^{-\rho}$ , are associated with incoming momenta  $p_1$ ,  $p_2$  and  $p_3$  respectively. They are:

$$O_{\varphi Q}^{(+)} : -\frac{e^3 v^2}{48\pi^2 s_W^2 \Lambda^2} \begin{cases} \epsilon^{\mu\nu\rho\sigma}(p_{2\sigma} - p_{3\sigma}) & \gamma \\ \epsilon^{\mu\nu\rho\sigma}(p_{3\sigma} - p_{1\sigma}) & W^+ \\ \epsilon^{\mu\nu\rho\sigma}(p_{1\sigma} - p_{2\sigma}) & W^- \end{cases} \quad (20)$$

$$O_{\varphi Q}^{(-)} : \frac{e^3 v^2}{48\pi^2 s_W^2 \Lambda^2} \begin{cases} \epsilon^{\mu\nu\rho\sigma}(p_{2\sigma} - p_{3\sigma}) & \gamma \\ \epsilon^{\mu\nu\rho\sigma}(p_{3\sigma} - p_{1\sigma}) & W^+ \\ \epsilon^{\mu\nu\rho\sigma}(p_{1\sigma} - p_{2\sigma}) & W^- \end{cases} \quad (21)$$

$$O_{tB} : \frac{3e^2 c_W v m_t}{8\sqrt{2}\pi^2 s_W^2 \Lambda^2} \begin{cases} 0 & \gamma \\ \epsilon^{\mu\nu\rho\sigma} p_{1\sigma} & W^+ \\ -\epsilon^{\mu\nu\rho\sigma} p_{1\sigma} & W^- \end{cases} \quad (22)$$

$$O_{tW} : \frac{e^2 v m_t}{8\sqrt{2}\pi^2 s_W \Lambda^2} \begin{cases} -3\epsilon^{\mu\nu\rho\sigma} (p_{2\sigma} - p_{3\sigma}) & \gamma \\ 2\epsilon^{\mu\nu\rho\sigma} (p_{1\sigma} - p_{2\sigma}) & W^+ \\ -2\epsilon^{\mu\nu\rho\sigma} (p_{1\sigma} - p_{3\sigma}) & W^- \end{cases} \quad (23)$$

The field after each line indicates the starting point of the trace. The other operators do not contribute.

This anomaly can be interpreted as the consequence of integrating out heavy chiral fermions. The anomaly free condition in the UV theory implies anomaly cancellation between different fermions. When matching to the SMEFT, if only some of them are integrated out, the resulting effective field theory could appear to be anomalous. However, when these chiral fermions are integrated out, they also generate a Wess-Zumino term which is supposed to cancel the gauge anomaly in the SMEFT. This term has the following form:

$$c_{WZ} \frac{e^3}{8\pi^2 s_W^2} \epsilon^{\mu\nu\rho\sigma} A_\mu \left( W_\nu^I \partial_\rho W_\sigma^I + \frac{1}{3} g_W \epsilon_{IJK} W_\nu^I W_\rho^J W_\sigma^K \right) \quad (24)$$

The coefficient of this term can be determined by requiring that the Ward identity for  $U(1)_{EM}$  is restored in the effective theory. Taking  $O_{\varphi Q}^{(+)}$  as an example, we first go to the consistent anomaly [61] by symmetrizing the anomaly with respect to all three external momenta. From Eq. (20), this corresponds to a vanishing R2 counterterm, and

$$p_1^\mu \Gamma_{\mu\nu\rho} = p_2^\mu \Gamma_{\rho\nu\mu} = p_3^\mu \Gamma_{\nu\rho\mu} = -\frac{C_{\varphi Q}^{(+)} e^3 v^2}{48\pi^2 s_W^2 \Lambda^2} \epsilon^{\nu\rho\alpha\beta} p_{2\alpha} p_{3\beta} \quad (25)$$

Then, the Wess-Zumino term gives an additional contribution

$$\Gamma_{\mu\nu\rho}^{WZ} = c_{WZ} \frac{e^3}{8\pi^2 s_W^2} \epsilon^{\mu\nu\rho\sigma} (p_{2\sigma} - p_{3\sigma}) \quad (26)$$

$$p_1^\mu \Gamma_{\mu\nu\rho}^{WZ} = 2c_{WZ} \frac{e^3}{8\pi^2 s_W^2} \epsilon^{\mu\nu\alpha\beta} p_{2\alpha} p_{3\beta} \quad (27)$$

For this to cancel the anomaly in Eq. (25), we need

$$c_{WZ} = \frac{C_{\varphi Q}^{(+)} v^2}{12\Lambda^2} \quad (28)$$

In our implementation, the contribution from this term can be added together with the R2 counterterms, leading to

$$R2_{O_{\varphi Q}^{(+)}}(WW\gamma) = \frac{C_{\varphi Q}^{(+)} e^3 v^2}{96\pi^2 s_W^2 \Lambda^2} \epsilon^{\mu\nu\rho\sigma} (p_{2\sigma} - p_{3\sigma}) \quad (29)$$

All three other operators can be dealt with in the same way. In practice, we note that this is equivalent to computing the trace by starting from  $W^+$  and  $W^-$  respectively, and then taking the average. Finally, we use the same prescription for the  $WWZ$  vertex.

## References

- 1 G. Aad *et al.* (ATLAS), *Observation of a new particle in the search for the Standard Model Higgs boson with the ATLAS detector at the LHC*, *Phys. Lett.* **B716** (2012) 1, arXiv:1207.7214 [hep-ex].
- 2 S. Chatrchyan *et al.* (CMS), *Observation of a new boson at a mass of 125 GeV with the CMS experiment at the LHC*, *Phys. Lett.* **B716** (2012) 30, arXiv:1207.7235 [hep-ex].
- 3 J. Ellis and T. You, *Sensitivities of Prospective Future  $e^+e^-$  Colliders to Decoupled New Physics*, *JHEP* **03** (2016) 089, arXiv:1510.04561 [hep-ph].
- 4 J. Ellis, P. Roloff, V. Sanz, and T. You, *Dimension-6 Operator Analysis of the CLIC Sensitivity to New Physics*, *JHEP* **05** (2017) 096, arXiv:1701.04804 [hep-ph].
- 5 G. Durieux, C. Grojean, J. Gu, and K. Wang, *The leptonic future of the Higgs*, *JHEP* **09** (2017) 014, arXiv:1704.02333 [hep-ph].
- 6 T. Barklow, K. Fujii, S. Jung, R. Karl, J. List, T. Ogawa, M. E. Peskin, and J. Tian, *Improved Formalism for Precision Higgs Coupling Fits*, *Phys. Rev.* **D97** (2018) 053003, arXiv:1708.08912 [hep-ph].
- 7 T. Barklow, K. Fujii, S. Jung, M. E. Peskin, and J. Tian, *Model-Independent Determination of the Triple Higgs Coupling at  $e^+e^-$  Colliders*, *Phys. Rev.* **D97** (2018) 053004, arXiv:1708.09079 [hep-ph].
- 8 S. Di Vita, G. Durieux, C. Grojean, J. Gu, Z. Liu, G. Panico, M. Riembau, and T. Vantalon, *A global view on the Higgs self-coupling at lepton colliders*, *JHEP* **02** (2018) 178, arXiv:1711.03978 [hep-ph].
- 9 W. H. Chiu, S. C. Leung, T. Liu, K.-F. Lyu, and L.-T. Wang, *Probing 6D operators at future  $e^-e^+$  colliders*, *JHEP* **05** (2018) 081, arXiv:1711.04046 [hep-ph].
- 10 M. McCullough, *An Indirect Model-Dependent Probe of the Higgs Self-Coupling*, *Phys. Rev.* **D90** (2014) 015001, [Erratum: *Phys. Rev.* D92, no.3, 039903(2015)], arXiv:1312.3322 [hep-ph].
- 11 G. Durieux, M. Perelló, M. Vos, and C. Zhang, *Global and optimal probes for the top-quark effective field theory at future lepton colliders*, arXiv:1807.02121 [hep-ph].
- 12 E. Vryonidou and C. Zhang, *Dimension-six electroweak top-loop effects in Higgs production and decay*, arXiv:1804.09766 [hep-ph].
- 13 C. Hartmann and M. Trott, *On one-loop corrections in the standard model effective field theory; the  $\Gamma(h \rightarrow \gamma\gamma)$  case*, *JHEP* **07** (2015) 151, arXiv:1505.02646 [hep-ph].
- 14 M. Ghezzi, R. Gomez-Ambrosio, G. Passarino, and S. Uccirati, *NLO Higgs effective field theory and  $\kappa$ -framework*, *JHEP* **07** (2015) 175, arXiv:1505.03706 [hep-ph].
- 15 C. Hartmann and M. Trott, *Higgs Decay to Two Photons at One Loop in the Standard Model Effective Field Theory*, *Phys. Rev. Lett.* **115** (2015) 191801, arXiv:1507.03568 [hep-ph].
- 16 R. Gauld, B. D. Pecjak, and D. J. Scott, *One-loop corrections to  $h \rightarrow b\bar{b}$  and  $h \rightarrow \tau\bar{\tau}$  decays in the Standard Model Dimension-6 EFT: four-fermion operators and the large- $m_t$  limit*, *JHEP* **05** (2016) 080, arXiv:1512.02508 [hep-ph].
- 17 S. Dawson and P. P. Giardino, *Higgs decays to ZZ and Z $\gamma$  in the standard model effective field theory: An NLO analysis*, *Phys. Rev.* **D97** (2018) 093003, arXiv:1801.01136 [hep-ph].
- 18 A. Dedes, M. Paraskevas, J. Rosiek, K. Suxho, and L. Trifylis, *The decay  $h \rightarrow \gamma\gamma$  in the Standard-Model Effective Field Theory*, (2018), arXiv:1805.00302 [hep-ph].
- 19 S. Dawson and P. P. Giardino, *Electroweak Corrections to*

- Higgs to  $\gamma\gamma$  and  $W^+W^-$  in the SMEFT*, [arXiv:1807.11504 \[hep-ph\]](#).
- 20 S. Weinberg, *Phenomenological Lagrangians, Proceedings, Symposium Honoring Julian Schwinger on the Occasion of his 60th Birthday: Los Angeles, California, February 18-19, 1978*, *Physica* **A96** (1979) 327.
  - 21 C. N. Leung, S. T. Love, and S. Rao, *Low-Energy Manifestations of a New Interaction Scale: Operator Analysis*, *Z. Phys.* **C31** (1986) 433.
  - 22 W. Buchmuller and D. Wyler, *Effective Lagrangian Analysis of New Interactions and Flavor Conservation*, *Nucl. Phys.* **B268** (1986) 621.
  - 23 C. Degrande, N. Greiner, W. Kilian, O. Mattelaer, H. Mebane, T. Stelzer, S. Willenbrock, and C. Zhang, *Effective Field Theory: A Modern Approach to Anomalous Couplings*, *Annals Phys.* **335** (2013) 21, [arXiv:1205.4231 \[hep-ph\]](#).
  - 24 S. Weinberg, *Effective Field Theory, Past and Future, Proceedings, 6th International Workshop on Chiral dynamics: Bern, Switzerland, July 6-10, 2009*, *PoS CD09* (2009) 001, [arXiv:0908.1964 \[hep-th\]](#).
  - 25 ATLAS Collaboration, *Study of the double Higgs production channel  $H(\rightarrow b\bar{b})H(\rightarrow \gamma\gamma)$  with the ATLAS experiment at the HL-LHC*, *ATL-PHYS-PUB-2017-001* (2017).
  - 26 C. Zhang, N. Greiner, and S. Willenbrock, *Constraints on Non-standard Top Quark Couplings*, *Phys. Rev.* **D86** (2012) 014024, [arXiv:1201.6670 \[hep-ph\]](#).
  - 27 M. E. Peskin and T. Takeuchi, *Estimation of oblique electroweak corrections*, *Phys. Rev.* **D46** (1992) 381.
  - 28 J. Alwall, R. Frederix, S. Frixione, V. Hirschi, F. Maltoni, O. Mattelaer, H. S. Shao, T. Stelzer, P. Torrielli, and M. Zaro, *The automated computation of tree-level and next-to-leading order differential cross sections, and their matching to parton shower simulations*, *JHEP* **07** (2014) 079, [arXiv:1405.0301 \[hep-ph\]](#).
  - 29 O. Mattelaer, *On the maximal use of Monte Carlo samples: reweighting events at NLO accuracy*, *Eur. Phys. J.* **C76** (2016) 674, [arXiv:1607.00763 \[hep-ph\]](#).
  - 30 D. Kreimer, *The  $\gamma(5)$  Problem and Anomalies: A Clifford Algebra Approach*, *Phys. Lett.* **B237** (1990) 59.
  - 31 J. G. Korner, D. Kreimer, and K. Schilcher, *A Practicable  $\gamma(5)$  scheme in dimensional regularization*, *Z. Phys.* **C54** (1992) 503.
  - 32 D. Kreimer, *The Role of  $\gamma_5$  in dimensional regularization*, (1993), [arXiv:hep-ph/9401354](#).
  - 33 A. Pomarol and F. Riva, *Towards the Ultimate SM Fit to Close in on Higgs Physics*, *JHEP* **01** (2014) 151, [arXiv:1308.2803 \[hep-ph\]](#).
  - 34 T. Corbett, O. J. P. Éboli, J. Gonzalez-Fraile, and M. C. Gonzalez-Garcia, *Determining Triple Gauge Boson Couplings from Higgs Data*, *Phys. Rev. Lett.* **111** (2013) 011801, [arXiv:1304.1151 \[hep-ph\]](#).
  - 35 A. Falkowski, M. Gonzalez-Alonso, A. Greljo, and D. Marzocca, *Global constraints on anomalous triple gauge couplings in effective field theory approach*, *Phys. Rev. Lett.* **116** (2016) 011801, [arXiv:1508.00581 \[hep-ph\]](#).
  - 36 J. Wess and B. Zumino, *Consequences of anomalous Ward identities*, *Phys. Lett.* **37B** (1971) 95.
  - 37 C. Patrignani et al. (Particle Data Group), *Review of Particle Physics*, *Chin. Phys.* **C40** (2016) 100001.
  - 38 J. D. Wells and Z. Zhang, *Effective theories of universal theories*, *JHEP* **01** (2016) 123, [arXiv:1510.08462 \[hep-ph\]](#).
  - 39 C. Degrande, J. M. Gerard, C. Grojean, F. Maltoni, and G. Servant, *Probing Top-Higgs Non-Standard Interactions at the LHC*, *JHEP* **07** (2012) 036, [Erratum: *JHEP*03,032(2013)], [arXiv:1205.1065 \[hep-ph\]](#).
  - 40 F. Maltoni, E. Vryonidou, and C. Zhang, *Higgs production in association with a top-antitop pair in the Standard Model Effective Field Theory at NLO in QCD*, *JHEP* **10** (2016) 123, [arXiv:1607.05330 \[hep-ph\]](#).
  - 41 CEPC-SPPC Study Group, *CEPC-SPPC Preliminary Conceptual Design Report. 1. Physics and Detector* (2015).
  - 42 M. Bicer et al. (TLEP Design Study Working Group), *First Look at the Physics Case of TLEP, Proceedings, 2013 Community Summer Study on the Future of U.S. Particle Physics: Snowmass on the Mississippi (CSS2013): Minneapolis, MN, USA, July 29-August 6, 2013*, *JHEP* **01** (2014) 164, [arXiv:1308.6176 \[hep-ex\]](#).
  - 43 M. Benedikt and F. Zimmermann, *Future Circular Collider Study: Status and Plans, FCC Week*, Amsterdam, 9 Apr 2018.
  - 44 M. J. Boland et al. (CLICdp, CLIC), *Updated baseline for a staged Compact Linear Collider*, [10.5170/CERN-2016-004, arXiv:1608.07537 \[physics.acc-ph\]](#).
  - 45 H. Baer, T. Barklow, K. Fujii, Y. Gao, A. Hoang, S. Kanemura, J. List, H. E. Logan, A. Nomerotski, M. Perelstein, et al., *The International Linear Collider Technical Design Report - Volume 2: Physics*, [arXiv:1306.6352 \[hep-ph\]](#).
  - 46 A. M. Sirunyan et al. (CMS), *Measurement of the  $t\bar{t}$  production cross section using events with one lepton and at least one jet in pp collisions at  $\sqrt{s} = 13$  TeV*, *JHEP* **09** (2017) 051, [arXiv:1701.06228 \[hep-ex\]](#).
  - 47 B. Schoenrock, E. Druke, B. Alvarez Gonzalez, and R. Schwienhorst, *Single top quark cross section measurement in the t-channel at the high-luminosity LHC*, in *Proceedings, 2013 Community Summer Study on the Future of U.S. Particle Physics: Snowmass on the Mississippi (CSS2013): Minneapolis, MN, USA, July 29-August 6, 2013*, [arXiv:1308.6307 \[hep-ex\]](#).
  - 48 M. Aaboud et al. (ATLAS), *Measurement of the W boson polarisation in  $t\bar{t}$  events from pp collisions at  $\sqrt{s} = 8$  TeV in the lepton + jets channel with ATLAS*, *Eur. Phys. J.* **C77** (2017) 264, [arXiv:1612.02577 \[hep-ex\]](#).
  - 49 ATLAS Collaboration, *Projections for measurements of Higgs boson signal strengths and coupling parameters with the ATLAS detector at a HL-LHC*, *ATL-PHYS-PUB-2014-016* (2014).
  - 50 E. L. Berger, J. Gao, C. P. Yuan, and H. X. Zhu, *NNLO QCD Corrections to t-channel Single Top-Quark Production and Decay*, *Phys. Rev.* **D94** (2016) 071501, [arXiv:1606.08463 \[hep-ph\]](#).
  - 51 A. Czarnecki, J. G. Korner, and J. H. Piclum, *Helicity fractions of W bosons from top quark decays at NNLO in QCD*, *Phys. Rev.* **D81** (2010) 111503, [arXiv:1005.2625 \[hep-ph\]](#).
  - 52 S. Di Vita, C. Grojean, G. Panico, M. Riemann, and T. Vantalon, *A global view on the Higgs self-coupling*, *JHEP* **09** (2017) 069, [arXiv:1704.01953 \[hep-ph\]](#).
  - 53 A. Azatov, R. Contino, G. Panico, and M. Son, *Effective field theory analysis of double Higgs boson production via gluon fusion*, *Phys. Rev.* **D92** (2015) 035001, [arXiv:1502.00539 \[hep-ph\]](#).
  - 54 M. Beneke, D. Boito, and Y.-M. Wang, *Anomalous Higgs couplings in angular asymmetries of  $H \rightarrow Z\ell^+\ell^-$  and  $e^+e^- \rightarrow HZ$* , *JHEP* **11** (2014) 028, [arXiv:1406.1361 \[hep-ph\]](#).
  - 55 N. Craig, J. Gu, Z. Liu, and K. Wang, *Beyond Higgs Couplings: Probing the Higgs with Angular Observables at Future  $e^+e^-$  Colliders*, *JHEP* **03** (2016) 050, [arXiv:1512.06877 \[hep-ph\]](#).
  - 56 O. Bessidskaia Bylund, F. Maltoni, I. Tsiniikos, E. Vryonidou, and C. Zhang, *Probing top quark neutral couplings in the Standard Model Effective Field Theory at NLO in QCD*, *JHEP* **05** (2016) 052, [arXiv:1601.08193 \[hep-ph\]](#).
  - 57 S. Boselli, R. Hunter, and A. Mitov, *Prospects for the determination of the top-quark Yukawa coupling at future  $e^+e^-$  colliders*, (2018), [arXiv:1805.12027 \[hep-ph\]](#).
  - 58 C. Shen and S.-h. Zhu, *Anomalous Higgs-top coupling pollution of the triple Higgs coupling extraction at a future high-luminosity electron-positron collider*, *Phys. Rev.* **D92** (2015) 094001, [arXiv:1504.05626 \[hep-ph\]](#).
  - 59 H. Abramowicz et al. (CLICdp), *Top-Quark Physics at the CLIC Electron-Positron Linear Collider*, [arXiv:1807.02441](#)

- 60 [\[hep-ex\]](#).  
R. Yonamine, K. Ikematsu, T. Tanabe, K. Fujii, Y. Kiyo, Y. Sumino, and H. Yokoya, *Measuring the top Yukawa coupling at the ILC at  $\sqrt{s} = 500$  GeV*, *Phys. Rev.* **D84** (2011)
- 61 [014033, arXiv:1104.5132 \[hep-ph\]](#).  
W. A. Bardeen and B. Zumino, *Consistent and Covariant Anomalies in Gauge and Gravitational Theories*, *Nucl. Phys.* **B244** (1984) 421